Journal of Superconductivity and Novel Magnetism (2019) 32:3415–3423
https://doi.org/10.1007/s10948-019-5127-z

ORIGINAL PAPER

The Effect of Zinc on the Structural, Electrical, and Mechanical Properties of YBCO-123 Superconducting Nanoparticles Prepared by an Acetate-Based Sol-Gel Process

E. Asikuzun[1,2] · O. Ozturk[2,3] · G. A. Aydemir[4] · A. T. Tasci[3]

Received: 22 March 2019 / Accepted: 25 April 2019 / Published online: 16 May 2019

Abstract
In this study, zinc (Zn)-doped YBaCuO (YBCO)-123-based high-temperature superconducting samples were produced using the sol-gel method, which is commonly used for preparing nanosize materials. Zn ions were substituted by Cu ions ($YBa_2Cu_{3-x}Zn_xO$), and Zn doping effects on structural, electrical, and mechanical properties of the YBCO-123 superconductors were examined in detail. Undoped sample was prepared under same conditions. X-ray diffraction analysis (XRD) was used to determine phase analysis and lattice parameters of the superconducting samples. To analyze the microstructure properties, scanning electron microscope (SEM) measurements were performed. Resistivity and microhardness measurements were also carried out for superconducting and mechanic properties, respectively. Vickers microhardness, young modulus, fracture toughness, and yield strength values of the samples were calculated. Microhardness measurements were analyzed using the Kick's law, proportional sample resistance (PSR) model, EPD model, the Hays-Kendall (HK) approach, and indentation-induced cracking (IIC) model.

Keywords YBCO · Zn · Sol-gel method · Superconducting · IIC model · XRD

1 Introduction

The critical transition temperature of the YBaCuO (YBCO) system, discovered by Wu in 1987, is 92 K [1], which is above the liquid nitrogen temperature (77 K). It is very important in terms of technological applications [2–7]. The YBCO-123 superconductor is associated with the number of metal atoms in the chemical formula of $YBa_2Cu_3O_{7-\delta}$ (YBCO).

Each YBCO unit cell is separated by a plane of yttrium atoms, and it has two CuO_2 planes between the two BaO planes. In the YBCO system, the crystal structure and conductivity characteristics of the system vary according to the amount of oxygen in the structure and the heat treatment temperature. This indicates that the system is structurally very sensitive to the amount of oxygen. $YBa_2Cu_3O_{7-\delta}$ is also expressed as YBCO-123 superconductor due to the number of metal atoms in the chemical formula. The symbol "δ" in the $YBa_2Cu_3O_{7-\delta}$ compound shows the oxygen deficiency. The system exhibits orthorhombic symmetry and superconductivity for $0 \le \delta \le 0.5$. The system passes from the orthorhombic phase (Fig. 1a) to the tetragonal phase (Fig. 1b) and loses its superconductivity property for $0.5 \le \delta \le 1$. The lattice parameters of $YBa_2Cu_3O_6$ system that has tetragonal symmetry ($a = b \neq c$) are $a = b = 3.85$ Å and $c = 11.83$ Å whereas the lattice parameters of $YBa_2Cu_3O_{6,95}$ system that has orthorhombic symmetry ($a \neq b \neq c$) are $a = 3.82$ Å, $b = 3.89$ Å, and $c = 11.7$ Å [8–10].

While working with YBCO materials, one of the most critical point to consider is to keep these materials away from moist air and water. This is because YBCO can interact with

✉ O. Ozturk
oozturk@kastamonu.edu.tr

1 Faculty of Engineering and Architecture, Department of Metallurgical and Materials Engineering, Kastamonu University, Kastamonu, Turkey

2 Research and Application Center, Kastamonu University, Kastamonu, Turkey

3 Faculty of Engineering and Architecture, Department of Electrical and Electronics Engineering, Kastamonu University, 37100 Kastamonu, Turkey

4 Institute of Science and Technology, Department of Physics, Kastamonu University, Kastamonu, Turkey

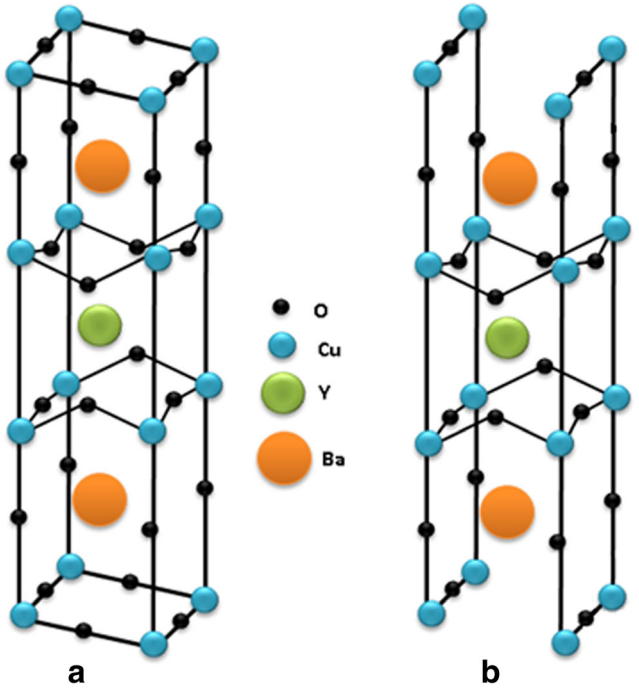

Fig. 1 a) Orthorhombic and b) Tetragonal crystal structures of the YBCO superconducting system

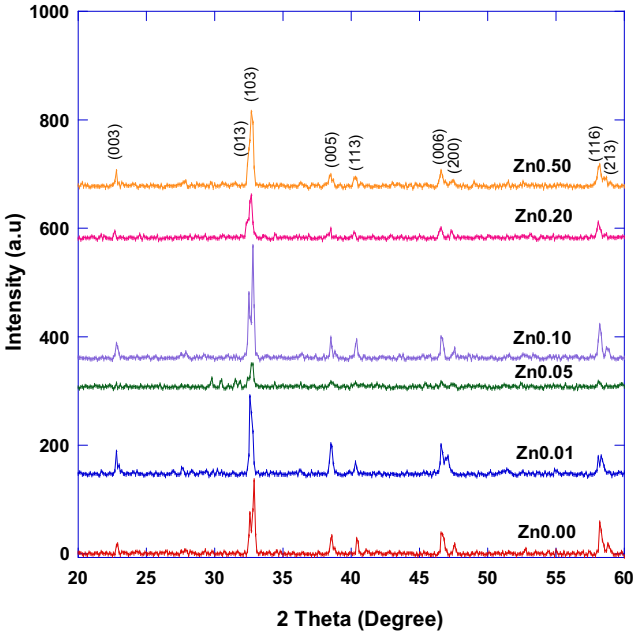

Fig. 2 XRD patterns of the samples

water and consequently transforms into a non-superconductor phase. Therefore, the YBCO materials should be stored in a dry environment to prevent dissolution [11, 12].

Mechanical properties are mainly specified with the interatomic bonding forces. In addition, with the internal structural modifications, the internal structure of the material and mechanical properties can be significantly improved. For mechanical characterization of materials, several parameters such as hardness, yield strength, elastic modulus, fracture toughness, and brittleness vary widely with different doping rates [13–16]. Determination of the mechanical properties of nanobulk materials is essential for many applications including glass materials for display, solar cells, liquid crystal displays, and heat mirrors.

With a combination of high strength and flexibility, the nanostructured materials represent the ideal materials for a wide variety of applications in aerospace and automotive industries, medicine, energy etc. Therefore, there has been an increasing interest on research regarding the mechanical properties of nanoparticles. Nanoparticle materials have different mechanical properties compared with microparticles and bulk materials [17, 18]. However, in order to develop these materials for high technology and to achieve progress in the fundamental science of nanostructures, it is crucial to understand the properties of these materials under different environments. There are many features that can vary significantly when the microstructure is nanoscale. The main aim of this study is to identify the mechanical properties of nanostructured materials including elastic properties, ductility and fracture toughness, and microhardness and strength.

In this study, Zn-doped YBCO-123 nanosamples were produced utilizing the sol-gel method. Structural, electrical, and mechanical properties of the obtained superconducting samples were examined in detail. DC resistivity measurement, XRD and SEM measurements, and Vickers microhardness test were carried out to determine the superconducting properties, crystal structure properties, phase formation, lattice parameters, surface morphology, and mechanical properties of the samples.

2 Experimental Details

In this study, the sol-gel method, which is widely preferred for preparation of the high-temperature superconductors, was used. Ten milliliters of acetic acid and 10 ml of methanol were added as solvent. Three grams of powder mixtures were prepared for each sample, and zinc acetate dihydrate were added at 1%, 5%, 10%,

Table 1 *a*, *b*, and *c* lattice parameters values of the samples

Samples	*a* (Å)	*b* (Å)	*c* (Å)
$Zn_{0.00}$	3.81	3.89	11.65
$Zn_{0.01}$	3.85	3.83	11.02
$Zn_{0.05}$	3.88	3.87	10.77
$Zn_{0.10}$	3.81	3.80	10.98
$Zn_{0.20}$	3.83	3.83	10.54
$Zn_{0.50}$	3.82	3.79	10.99

20%, and 50% of the powder. Beakers were closed, and the precursors and solvents were stirred at 60 ° C for 8 h using a heater magnetic stirrer until a transparent solution was obtained. Next, the beakers were opened and solutions were evaporated at 60 ° C using the heater magnetic stirrer until a gelation was observed. Finally, gelations were preheated at 300 ° C for 30 min in air using a muffle furnace. Following this process, powders were obtained for calcination process. The powder samples were calcined 3 times at 850 °C for 24 h. The produced samples were named as $Zn_{0.00}$, $Zn_{0.01}$, $Zn_{0.05}$, $Zn_{0.10}$, $Zn_{0.20}$, and $Zn_{0.50}$ depending on the Zn doping ratio undoped (i.e., 1%, 5%, 10%, 20% and 50%).

XRD measurements were performed by a Bruker D8 Advance X-ray powder diffractometer using Cu-K_α radiation in the range of $3° \leq 2\theta \leq 90°$ at a scan speed of 2°/min. Surface morphology of samples were performed using a Quanta FEG 250 scanning electron microscopy. The electrical properties of the samples were examined by DC resistivity against temperature measurements using 5 mA DC current through the samples at a temperature range of 20 to 150 K in a Janis brand closed-cycle cryostat. In order to reduce contact resistance, both voltage and current contacts were generated with silver paint contact. A Keithley 220 programmable current source and a Keithley 2182A nanovoltmeter system were used for the conventional four-probe measurements. The mechanical characterizations of samples were carried out using a Shimadzu brand HMV-2 model digital static microhardness tester.

3 Analyses and Obtained Results

3.1 XRD and SEM Analyses of Superconducting Nanoparticles

The XRD patterns of the $Zn_{0.00}$, $Zn_{0.01}$, $Zn_{0.05}$, $Zn_{0.10}$, $Zn_{0.20}$, and $Zn_{0.50}$ samples were given in Fig. 2. According to the XRD graph, the dominant phase examined in the undoped and Zn-doped samples was YBCO-123 phase. No peaks

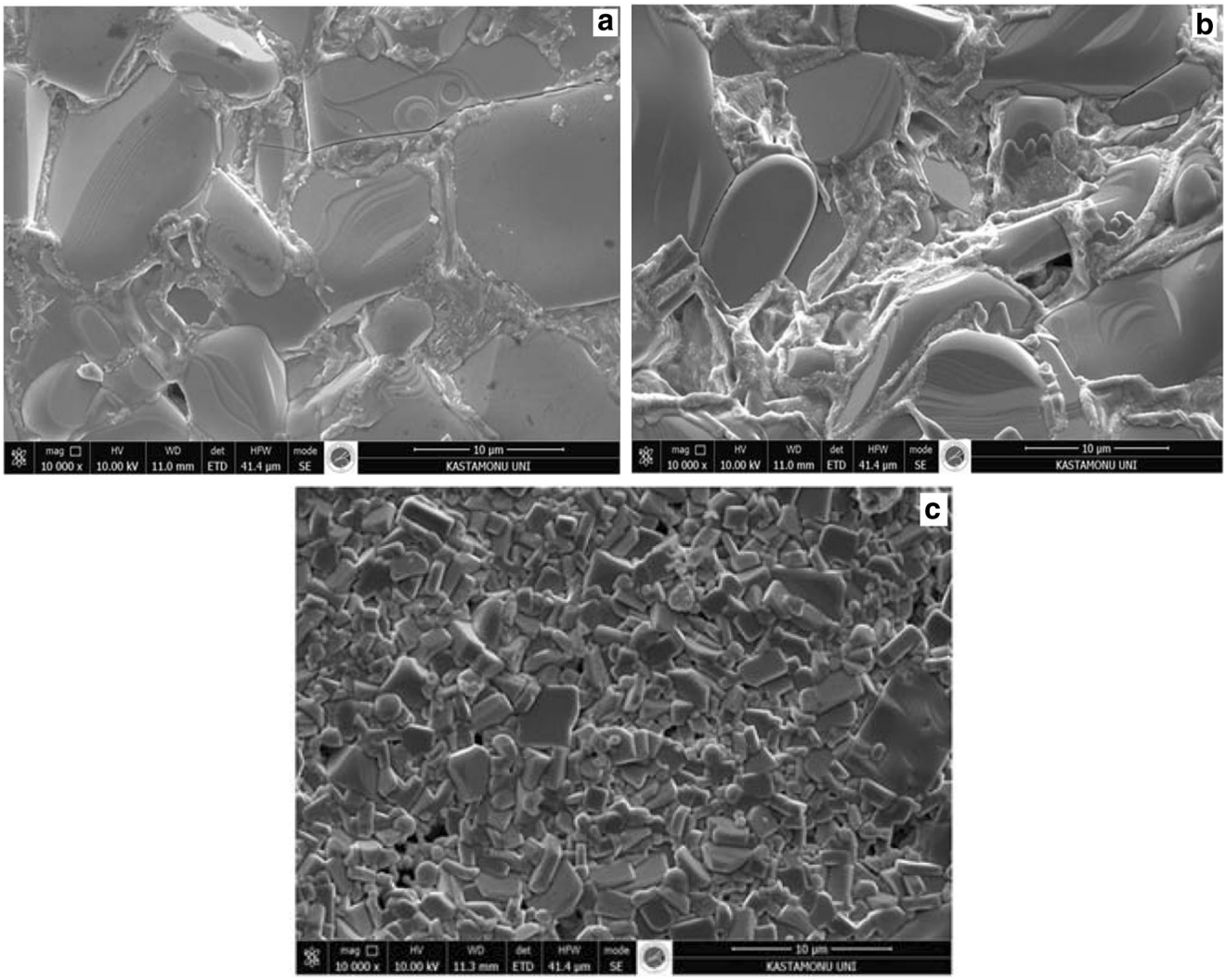

Fig. 3 SEM images of $Zn_{0.00}$, $Zn_{0.01}$, and $Zn_{0.50}$ of the samples

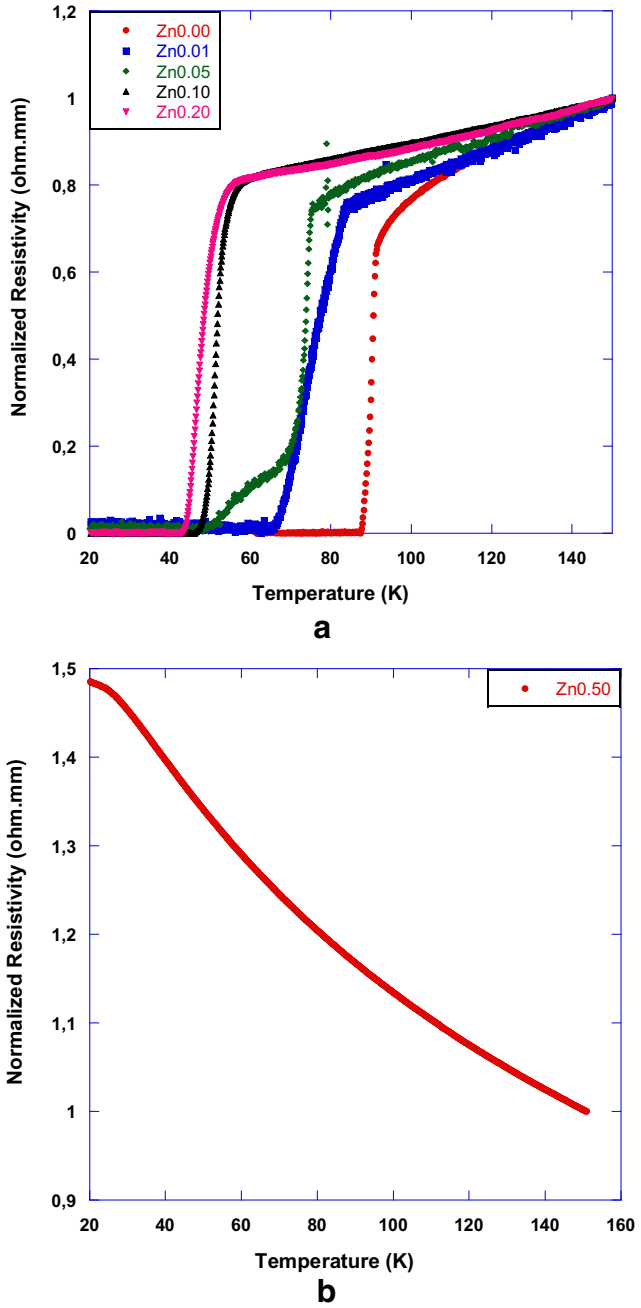

Fig. 4 Normalized resistivity as a function of temperature curves for the samples

related to Zn ion were observed from Fig. 2. The fact that the ionic radius of the Cu^{+2} (0.73 Å) ion is comparable with the ionic radius of the doped Zn^{+2} (0.74 Å) suggests that this substitution seems to be acceptable [19].

The lattice parameters *a*, *b*, and *c* of all samples were calculated, and given in Table 1. Table 1 indicates that the *a* lattice parameter of the samples increased up to the $Zn_{0.05}$ doping and decreased after reaching this value, while *c* lattice parameter decreased up to the $Zn_{0.05}$ doping and then increased. This result explains that the doping rate of 0.05 is a

Table 2 Variation of T_c and ΔT_c of the samples

Samples	Critical temperature		ΔT_c (*K*) $(T_c^{onset} - T_c^{offset})$
	$T_c^{offset}(K)$	$T_c^{onset}(K)$	
$Zn_{0.00}$	87	89	2
$Zn_{0.01}$	65	84	19
$Zn_{0.05}$	48	75	27
$Zn_{0.10}$	46	56	10
$Zn_{0.20}$	42	54	12

threshold value, and the structure of the sample varies slightly at all doping rates after this value. Peak intensities first decreased and increased afterwards until the $Zn_{0.05}$ doping rate is reached. In the literature, the lattice parameters of YBCO-123 system having orthorhombic symmetry ($a \neq b \neq c$) are a = 3.82 Å, b = 3.89 Å, and c = 11.7 Å. Our findings show that the lattice parameters of Zn-doped samples produced in this study are consistent with the literature data. When the crystal structure was examined, the increase in the *x* and *y* axes, associated with the *a* and *b* lattice parameters, causes a decrease in the *c* lattice parameter along the *z* axis (Table 1).

SEM analyses were performed in order to examine the surface morphology, grain size, and accumulation in grain boundaries of Zn-doped YBCO-123 system. In Fig. 3, SEM images of $Zn_{0.00}$, $Zn_{0.01}$ and $Zn_{0.50}$ samples were given at 10000 magnification. According to the results, the grain sizes decreased and porosity increased with increasing Zn doping. When $Zn_{0.00}$ and $Zn_{0.50}$ samples were compared, it was found that grains of $Zn_{0.50}$ sample were smaller, and the surface of the sample was more porous. In

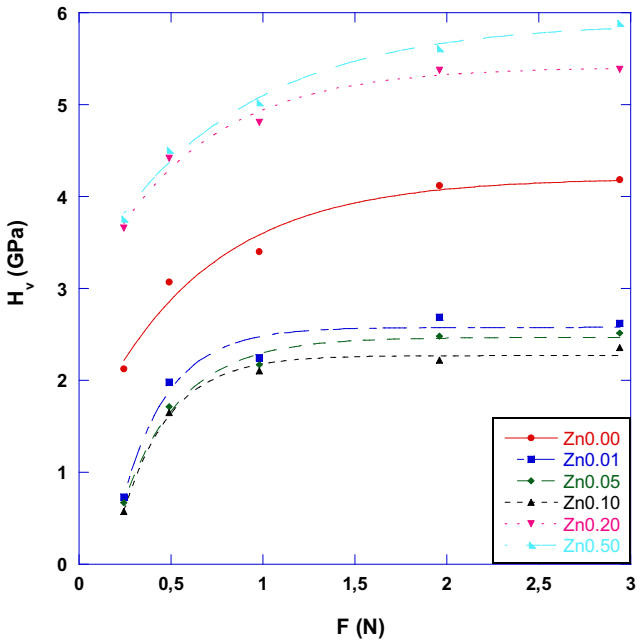

Fig. 5 Microhardness values as a function of the applied load

Table 3 H_v, E, K_{IC}, and Y values of the samples

Samples	F (N)	H_v (GPa)	E (GPa)	Y (GPa)	K_{ic} ($Pa/m^{1/2}$)
$Zn_{0.00}$	0.245	2.126	174.27	0.708	− 2.963
	0.490	3.073	251.92	1.024	− 3.563
	0.980	3.401	278.78	1.133	− 3.748
	1.960	4.121	337.84	1.373	− 4.126
	2.940	4.186	343.11	1.395	− 4.158
$Zn_{0.01}$	0.245	0.728	59.72	0.242	− 1.867
	0.490	1.979	162.23	0.659	− 3.078
	0.980	2.245	184.08	0.748	− 3.278
	1.960	2.687	220.30	0.895	− 3.586
	2.940	2.621	214.87	0.873	− 3.542
$Zn_{0.05}$	0.245	0.672	55.10	0.224	− 1.889
	0.490	1.715	140.56	0.571	− 3.017
	0.980	2.173	178.14	0.724	− 3.397
	1.960	2.478	203.12	0.826	− 3.627
	2.940	2.513	205.99	0.837	− 3.653
$Zn_{0.10}$	0.245	0.576	47.21	0.192	− 1.332
	0.490	1.651	135.32	0.550	− 2.255
	0.980	2.105	172.54	0.701	− 2.547
	1.960	2.224	182.28	0.741	− 2.617
	2.940	2.360	193.43	0.786	− 2.696
$Zn_{0.20}$	0.245	3.658	299.85	1.219	− 3.058
	0.490	4.416	362.02	1.472	− 3.360
	0.980	4.808	394.10	1.602	− 3.506
	1.960	5.377	440.72	1.792	− 3.708
	2.940	5.385	441.38	1.795	− 3.710
$Zn_{0.50}$	0.245	3.753	307.64	1.251	− 3.507
	0.490	4.503	369.09	1.501	− 3.842
	0.980	5.019	411.44	1.673	− 4.056
	1.960	5.608	459.69	1.869	− 4.288
	2.940	5.882	482.16	1.960	− 4.391

addition, plate-like structures commonly observed in the YBCO-123 high-temperature superconductors were observed in the undoped and Zn-doped samples.

3.2 Electrical Resistivity Analyses of Superconducting Nanoparticles

The resistivity of the samples as a function of temperature was measured, and onset transition temperatures (T_c^{onset}) of the samples were determined as the transition temperature from normal state to superconducting state.

The variation of resistivity with temperature was given in Fig. 4 for all samples. Findings indicate that all samples show metallic behavior above T_c^{onset} temperature. T_c^{onset} was 89 K for the undoped sample, while it was 84 K, 75 K, 56 K, and 54 K for $Zn_{0.01}$, $Zn_{0.05}$, $Zn_{0.10}$, and $Zn_{0.20}$ samples, respectively. The $Zn_{0.50}$ sample exhibited

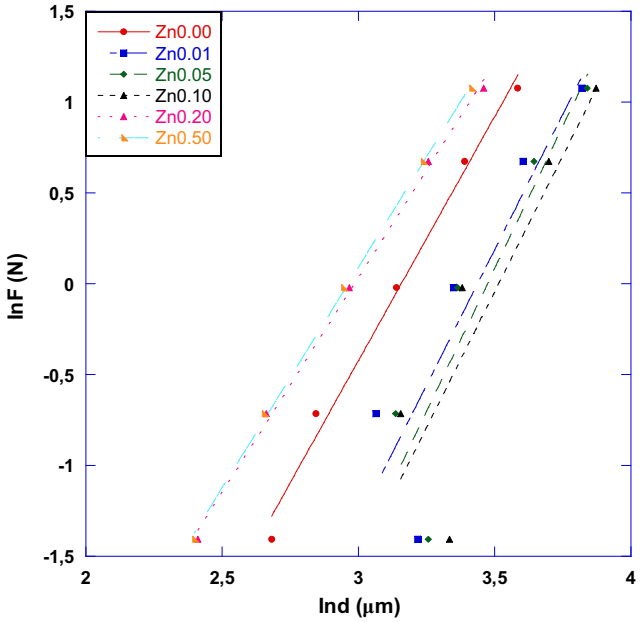

Fig. 6 Plots of ln$F$ versus ln$d$ of the samples

an insulative behavior (Fig. 4b). These results showed that the transition temperature (T_c^{onset}) to superconductivity decreased with Zn doping (Fig. 4a).

According to the resistivity-temperature change, it was observed that there was a double step only on the $Zn_{0.50}$ sample. This transition can be associated with the presence of impurity phases which cause a weak link at grain boundaries [20]. It was found that room temperature resistivity increased with increasing the Zn doping. Moreover, the grain size decreased with Zn doping, while the contact points of the grains increased with decreasing grain size that also caused an increase in resistivity. As shown in Fig. 4, the transition temperature width (ΔT_c) increased in the doped samples when it was compared with the undoped sample (Table 2). This was likely due to the fact the impurity levels and the lattice defects of the doped samples [21].

Table 4 Experimental data according to Meyer Law and PSR model

Samples	Meyer number n	$\alpha\ x10^{-2}$ (N)	$\beta\ x10^{-4}$ (N/μm)	H_{PSR} (GPa)	H_v (GPa)
$Zn_{0.00}$	2.68	− 2.52	29.93	5.550	4.121–4.186
$Zn_{0.01}$	2.98	− 2.92	21.07	3.907	2.621–2.687
$Zn_{0.05}$	3.14	− 3.24	20.96	3.886	2.478–2.513
$Zn_{0.10}$	2.99	− 1.88	18.85	3.495	2.224–2.360
$Zn_{0.20}$	2.36	− 1.56	34.31	6.362	2.377–5.385
$Zn_{0.50}$	2.42	− 2.00	38.16	7.076	5.608–5.882

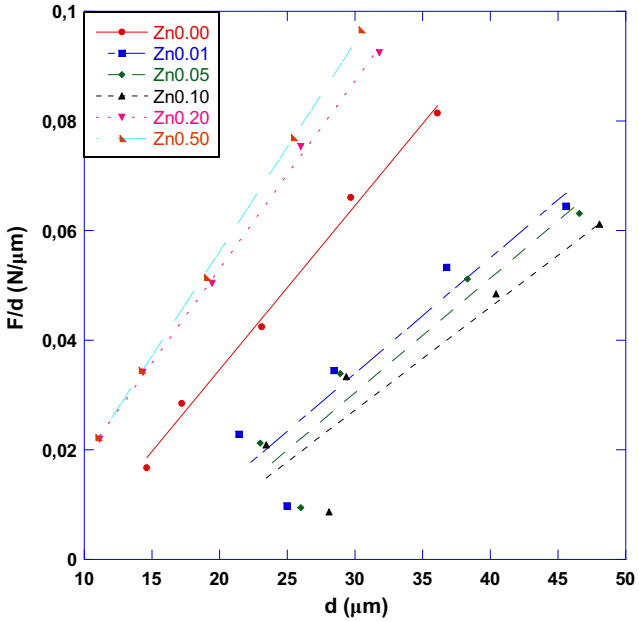

Fig. 7 Plots of F/d versus d of the samples

3.3 Vickers Microhardness Analyses of Superconducting Nanoparticles

The Vickers microhardness test was developed to measure the hardness of materials. This test has one of the widest scales among the hardness tests, and it can be used for all materials. Different loads were applied in the range of 0.245–2.940 N for 10 s on the surface of the samples, and the Vickers microhardness values (H_v) were calculated using the Eq. 1.

$$H_v = \frac{1854.4\ F}{d^2}\ GPa \tag{1}$$

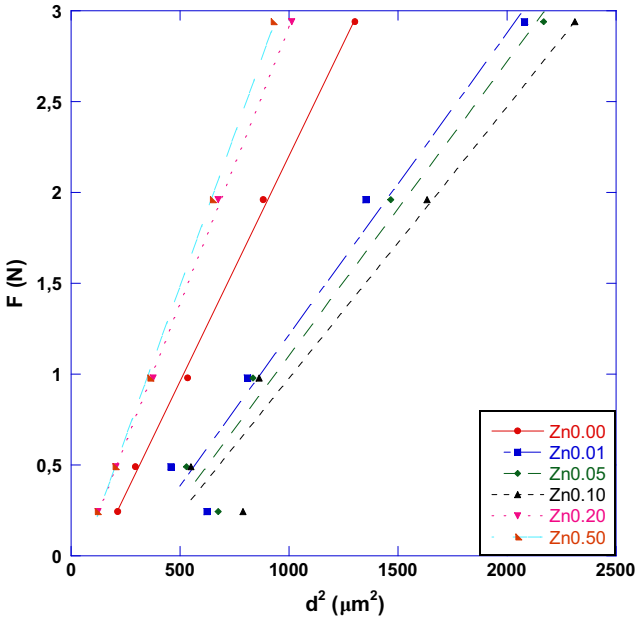

Fig. 8 Plots of F versus d^2 of the samples

where F is applied load on the surface of material, and d is the diagonal length of trace that is formed indenter.

The variation of the load dependent microhardness values as a function of the test loads were shown in Fig. 5. While the microhardness values decreased for $Zn_{0.01}$, $Zn_{0.05}$, and $Zn_{0.10}$ superconducting samples, they increased for $Zn_{0.20}$ and $Zn_{0.50}$ samples (Table 3, Fig. 5). The observed reduction is related to impurity phases as well as irregularity of the crystal structure. These factors lead to weakening of the strong bonds and reduction in microhardness. The observed increase is associated with Zn atoms between intergranulars. It is likely that Zn atoms penetrated between the grains after 20% doping rate.

Furthermore, the microhardness values increased with applied load [22, 23]. This nonlinear case is known as reverse indentation size effect (RISE) in the literature [24–27]. A smaller indentation load shows a smaller hardness value. As can be seen from Fig. 5, all samples exhibited a RISE behavior. In addition, it was observed that the microhardness values reached a plateau (saturation region) at around 1.5 N for all samples. In this study, material behavior was unchanged, but only microhardness values changed with Zn doping.

There are many models developed for analyzing the microhardness of materials in the literature [28, 29]. These models have been used to determine the behavior (ISE or RISE) of these materials against the applied load for mechanical characterizations.

In this study, parameters such as elastic modulus (E), yield strength (Y), and fracture toughness (K_{IC}), which are considered as important as the hardness of the mechanical characterizations of materials, were also calculated. The values of these parameters were given in Table 3 indicating that E, Y, and K_{IC} values, which are related with hardness, changed with Zn doping.

3.3.1 Meyer Law and PSR Model

The ISE (indentation size effect) or RISE (reverse indentation size effect) behavior of materials can be explained by Meyer's law:

$$F = Kd^n \tag{2}$$

where F, d, n, and K are applied load, diagonal length, Meyer index and constant, respectively. For analysis of this model, InF-Ind graph (Fig. 6) was drawn. The slope of the graph gives the value of n for Meyer's law and we can see that n values were found to be greater than 2 for each sample in this study. As a result, according to Meyer's law, all samples exhibited a RISE behavior (Table 4). It is recommended that $n > 2$ means a RISE behavior while $n < 2$ refers to an ISE behavior.

Eq. 3 was used for the proportional sample resistance (PSR) model. The α is the value where $(F/d) - d$ axis intersected (Fig. 7), and β is the slope of the line:

$$F/d = \alpha + \beta d \tag{3}$$

Table 5 Experimental data according to HK approach and IIC model

Samples	A_{HK} $x10^{-4}$ (GPa)	W_{HK} (N)	H_{HK} (GPa)	m	H_{IIC} (GPa)	H_v (GPa)
$Zn_{0.00}$	24.84	− 0.27	4.606	0.47	3.581	4.121–4.186
$Zn_{0.01}$	16.62	− 0.44	3.082	0.56	1.547	2.621–2.687
$Zn_{0.05}$	28.89	− 0.62	5.357	0.56	2.944	2.478–2.513
$Zn_{0.10}$	14.95	− 0.51	2.772	0.56	3.732	2.224–2.360
$Zn_{0.20}$	30.58	− 0.14	5.670	0.39	4.883	2.377–5.385
$Zn_{0.50}$	33.52	− 0.19	6.215	0.41	4.981	5.608–5.882

In this model, load-independent microhardness values were calculated with the Eq. (4):

$$H_{PSR} = 1854.4\beta \tag{4}$$

The α values of the samples were negative (Table 4). Negative α value confirms that the character of the behavior of these materials is in the form of a RISE behavior. This indicates that only plastic deformation is present in all samples without elastic deformation. Finally, given the comparison of H_{PSR} hardness values with the value that corresponds to the plateau region, it can be clearly seen that these microhardness values were quite far from the plateau region (Table 4) [29]. Therefore, it is clear that the PSR model is insufficient to determine the true microhardness values for samples showing a RISE behavior.

3.3.2 HK Approach and IIC Model

Hays and Kendall suggested that minimum load value (W) can create permanent deformation in a sample [30]. According to the HK approach, if the applied load does not exceed this resistance, permanent deformation does not occur and only elastic deformation occurs. Based on the HK approach, W_{HK} and A_{1HK}values were calculated from $F-d^2$ graph. A_{1HK} is a constant independent from the applied load.

$$F-W_{HK} = A_{HK}d^2 \tag{5}$$

In addition, independent of the load, the microhardness value was calculated using Eq. 6 below:

$$H_{HK} = 1854.4A_{HK} \tag{6}$$

At the same time, according to the IIC model, the applied test load is offset by the total resistance of the sample at maximum depth, whereas the friction and elastic effects led to normal ISE behavior and indentation cracks led to RISE behavior.

$\ln(H_v)$-$\ln(F^{5/3}/d^3)$ graph (Fig. 9) was drawn according to the IIC model. K and m values were independent of load, and they were calculated from the graph. The microhardness values of the samples were calculated using Eq. 7.

$$H_v = K\left(\frac{F^{5/3}}{d^3}\right)^m \tag{7}$$

When HK approach and indentation-induced cracking (IIC) model was analyzed, the following results were obtained.

- A negative W_{HK} value obtained according to the HK approach suggests that applied load is sufficient to produce plastic deformation, but insufficient for elastic deformation. The microhardness values calculated by the HK model using Fig. 8 were quite far from the plateau region (Table 5). As a result, the HK model seems to be unsuccessful to determine the true microhardness values.
- The m index obtained according to the IIC model (Fig. 9) was used to explain ISE or RISE behaviors [31–33]. Given Table 5, the value of m was found to be less than 0.6. According to this result, we can conclude that the

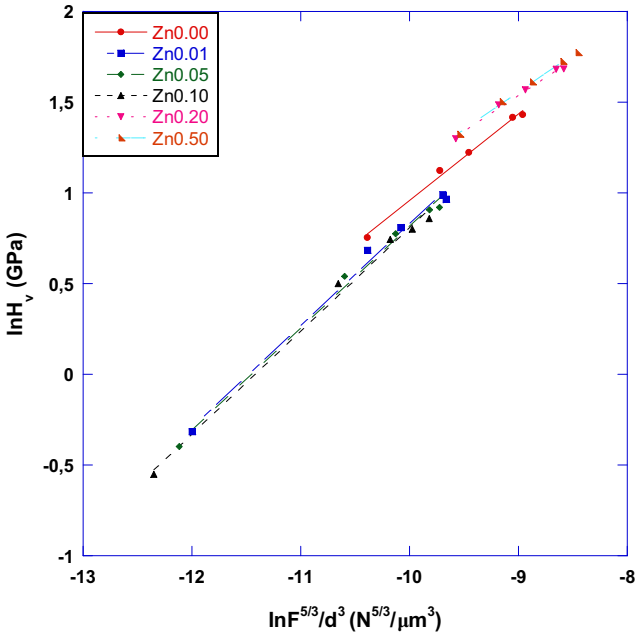

Fig. 9 Plots of $\ln H_v$ versus $\ln(F^{5/3}/d^3)$ of the samples

samples exhibited a RISE behavior. Since no elastic deformation was observed in the samples, this model would be the most successful model for samples showing the RISE behavior.

4 Conclusions

In this study, Zn-doped YBCO-123-based high-temperature superconducting samples were produced using the sol-gel method. The structural, electrical, and mechanical properties of the superconducting samples were examined in detail. The obtained results are summarized below:

- According to the XRD results, a second phase which caused a remarkable change and a peak belonging to the Zn ion were not found in the diffraction patterns. This finding showed that most of the Zn atoms were located in the YBCO-123 matrix.
- *a* and *b* lattice parameters increased until $Zn_{0.05}$, and then decreased. However, *c* lattice parameter decreased until $Zn_{0.05}$ and increased afterwards. This result explained that the 0.05 doping rate was a threshold value because the structure changed slightly after this doping.
- According to the SEM results, it was observed that grain sizes decreased and porosity increased with increasing Zn doping. When $Zn_{0.00}$ and $Zn_{0.50}$ samples were compared, it was observed that grains of the $Zn_{0.50}$ sample were smaller and the surface of the sample was more porous.
- The ρ-T measurements showed that room temperature resistivity increased with increasing Zn doping.
- The superconducting transition width, ΔT_c, was increased when compared with the undoped sample. This may be due to the higher impurity level and lattice defects of the Zn-doped samples.
- The T_c^{offset} were 87 *K*, 65 *K*, 48 *K*, 46 *K*, and 42 *K* for the samples $Zn_{0.00}$, $Zn_{0.01}$, $Zn_{0.05}$, $Zn_{0.10}$, and $Zn_{0.20}$, respectively. The T_c^{onset} was found as 89 *K* for undoped sample. The transition temperatures to superconductivity were 84 *K*, 75 *K*, 56 *K* and 54 *K* for $Zn_{0.01}$, $Zn_{0.05}$, $Zn_{0.10}$, and $Zn_{0.20}$ samples, respectively. As a result, the superconducting transition temperature (T_c^{onset}) decreased with increasing Zn doping.
- The microhardness value increased with increasing applied load on the surface of the sample, which means that the sample showed the RISE behavior. The calculated microhardness value increased rapidly with increasing load up to 1.5 N and remained nearly constant thereafter.
- When the microhardness models were analyzed, the most suitable model for the Zn-doped YBCO-123 superconducting samples exhibiting the RISE behavior was determined as the IIC model.

Funding Information This study was supported by the Kastamonu University Scientific Research Projects Coordination Department under the Grant No. KÜ-BAP01/2016-21. Besides, we also thank the Kastamonu University Research and Application Center for the supports.

References

1. Tarascon, J.M., McKinnon, W.R., Barboux, P., Hwang, D.M., Bagley, B.G., Greene, L.H.: Preparation, structure, and properties of the superconducting compound series $Bi_2Sr_2Ca_{n-1}Cu_nO_y$ with n=1, 2 and 3. Phys. Rev. B. **38**, 2504 (1988)
2. Tosun, M., Ataoglu, S., Arda, L., Ozturk, O., Asikuzun, E., Akcan, D., Çakıroglu, O.: Structural and mechanical properties of *ZnMgO* nanoparticles. J. Mater. Sci. Eng. A. **590**, 416–422 (2014)
3. Fossheim, K., Sudbo, A.: Superconductivity Physics and Applications, pp. 37–39. John Wiley & Sons, England (2004)
4. Gaganidze, E., Halbritter, J.: Morphology and transport properties of Ca-doped superconducting epitaxial YBCO films. Supercond. Sci. Technol. **17**, 1346–1352 (2004)
5. Abraham Godlyn, A., Manikandan, A., Manikandan, E., Jaganathan, S.K., Baykal, A., Renganathan, S.P.: Enhanced opto-magneto properties of $Ni_xMg_{1-x}Fe_2O_4$ ($0.0 \leq x \leq 1.0$) ferrites nano-catalysts. J. Nanoelectron. Optoelectron. **12**, 1326–1333 (2017)
6. Slimani, Y., Baykal, A., Manikandan, A.: Effect of Cr^{3+} substitution on AC susceptibility of Ba hexaferrite nanoparticles. J. Magn. Magn. Mater. **458**, 204–212 (2018)
7. Asiri, S., Sertkol, M., Guner, S., Gungunes, H., Batoo, K.M., Salehf, T.A., Sozerig, H., Almessierea, M.A., Manikandanh, A., Baykal, A.: Hydrothermal synthesis of $Co_yZn_yMn_{1-2y}Fe_2O_4$ nanoferrites: magneto-optical investigation. Ceram. Int. **44**, 5751–5759 (2018)
8. Hott, R., Rietschel, H.: Applied Superconductivity Status Report Forschungszentrum Karlsruhe. (1988)
9. Putilin, S.N., Antipov, E.V., Chmaissen, O., Marezio, M.: Superconductivity at 94 *K* in $HgBa_2CuO_{4+d}$. Nature. **362**, 226 (1993)
10. Saxena, A.K.: High-Temperature Superconductors, pp. 123–210. Springer Heidelberg Dordecht, New York (2010)
11. Silambarasu, A., Manikandan, A., Balakrishnan, K.: Room-temperature superparamagnetism and enhanced photocatalytic activity of magnetically reusable spinel $ZnFe_2O_4$ nanocatalysts. J. Supercond. Nov. Magn. **30**, 2631–2640 (2017)
12. Hema, E., Manikandan, A., Gayathri, M., Durka, M., Antony Arul, S., Venkatraman, B.R.: The role of Mn^{2+}-doping on structural, morphological, optical, magnetic and catalytic properties of spinel $ZnFe_2O_4$nanoparticles. J. Nanosci. Nanotechnol. **16**, 5929–5943 (2016)
13. Siddheswaran, R., Mangalaraja, R.V., Avila, R.E., Manikandan, D., Jeyanthi, C.E., Ananthakumar, S.: Evaluation of mechanical hardness and fracture toughness of co and Al co-doped ZnO. Mat. Sci. Eng. A. **558**, 456–461 (2012)
14. Rajkovic, V., Bozic, D., Devecerski, A., Jovanovic, M.T.: Characteristic of copper matrix simultaneously reinforced with nano-and micro-sized Al_2O_3 particles. Mater. Charact. **67**, 129–137 (2012)
15. Shun, T.T., Chang, L.Y., Shiu, M.H.: Microstructure and mechanical properties of multiprincipal component $CoCrFeNiMo_x$ alloys. Mat.Charac. **70**, 63–67 (2012)
16. Arda, L., Ozturk, O., Asikuzun, E., Ataoglu, S.: Structural and mechanical properties of transition metals doped ZnMgO nanoparticles. Powder Technol. **235**, 479–484 (2013)
17. Maria Lumina Sonia, M., Anand, S., Maria Vinosel, V., Asisi Janifer, M., Pauline, S., Manikandan, A.: Effect of lattice strain on structure, morphology and magneto-dielectric properties of

spinel $NiGd_xFe_{2-x}O_4$ ferrite nano-crystallites synthesized by sol-gel route. J. Magn. Magn. Mater. **466**, 238–251 (2018)
18. Asiri, S., Sertkol, M., Güngüneş, H., Amir, M.D., Manikandan, A., Ercan, I., Baykal, A.: The temperature effect on magnetic properties of $NiFe_2O_4$ nanoparticles. J. Inorg. Organomet. Polym. Mater. **28**, 1587–1597 (2018)
19. Asikuzun, E.: Production procedure and characterization of Zn-doped Y-123 superconducting samples prepared by sol-gel method. J. Supercond. Nov. Magn. **31**, 3509–3514 (2018)
20. Josephson, B.D.: Possible new effects in superconductive tunneling. Phys. Lett. **1**, 251–253 (1962)
21. Pippard, A.B.: The coherence concept in superconductivity. Physica. **19**, 765–774 (1953)
22. Tosun, M., Ataoğlu, S., Arda, L., Öztürk, Ö., Aşıkuzun, E., Akcan, D., Çakıroğlu, O.: Structural and mechanical properties of ZnMgO nanoparticles. J. Mater. Sci. Eng. A. **590**, 416–422 (2014)
23. Ozturk, O., Cetinkara, H.A., Asikuzun, E., Akdogan, M., Yilmazlar, M., Terzioglu, C.: Investigation of mechanical and superconducting properties of iron diffusion-doped Bi-2223 superconductors. J. Mater. Sci. Mater. Electron. **22**, 1501–1508 (2011)
24. Polinger, V., Haskel, D., Stern, E.A.: John-Teller Impurity States in LaSrCuO:XAFS Evidence and Implications for High T_c Superconductivity. (1998)
25. Bednorz, J.G., Müller, K.A.: Possible high T_c superconductivity in the Ba−La−cu−O system. Z. Phys. B. **64**, 189–193 (1986)
26. Sheng, Z.Z., Hermann, A.M.: Superconductivity in the rare-earth-free Tl_δ-Ba_δ-$Cu_{d\text{-}O}$ system above liquid-nitrogen tempature. Nature. **332**, 55 (1988)
27. Kumakura, H., Togano, K., Uehara, M., Maeda, H., Takahasni, K., Nakao, M.: Properties and Microstructure of Sintered High-T_c Bi-Sr-Ca-Cu-O and Tl-Ca-Ba-Cu-O Oxides. IEEE Transact. Magn. **25**, 2546–2549 (1989)
28. Sangwal, K.: On the reverse indentation size effect and microhardness measurement of solids. Mater. Chem. Phys. **63**, 145–152 (2000)
29. Rose-Innes, A.C., Rhoderic, E.H.: Introduction to superconductivity. New York Pergamon. **5 (**1978)
30. Hays, C., Kendall, E.G.: An analysis of Knoop microhardness. Metallography. **6**, 275–282 (1973)
31. Bull, S.J., Page, T.F., Yoffe Philos, E.H.: An explanation of the indentation size effect in ceramics. Mag. Lett. **59**, 281–288 (1989)
32. Awad, R., Abou Aly, A.I., Kamal, M., Anas, M.: Mechanical properties of $(Cu_{0.5}Tl_{0.5})$-1223 substituted by Pr. J. Supercond. Nov. Magn. **24**, 1947–1956 (2011)
33. Gong, J., Wu, J., Guan, Z.: Examination of the indentation size effect in low-load vickers hardness testing of ceramics. J. Eur. Ceram. Soc. **19**, 2625–2631 (1999)